View metadata, citation and similar papers at core.ac.uk

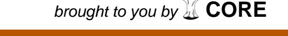

provided by DepositOnce

COMMUNICATIONS PHYSICS

ARTICLE

DOI: 10.1038/s42005-018-0044-1 OPEN

Suppression of the quantum-confined Stark effect in polar nitride heterostructures

S. Schlichting[1], G.M.O. Hönig[2], J. Müßener[3], P. Hille[3], T. Grieb[3], S. Westerkamp[1], J. Teubert[4], J. Schörmann[4], M.R. Wagner[1], A. Rosenauer[3], M. Eickhoff[3], A. Hoffmann[1] & G. Callsen[1,5]

Recently, we suggested an unconventional approach (the so-called Internal-Field-Guarded-Active-Region Design "IFGARD") for the elimination of the quantum-confined Stark effect in polar semiconductor heterostructures. The IFGARD-based suppression of the Stark redshift on the order of electronvolt and spatial charge carrier separation is independent of the specific polar semiconductor material or the related growth procedures. In this work, we demonstrate by means of micro-photoluminescence techniques the successful tuning as well as the elimination of the quantum-confined Stark effect in strongly polar [000-1] wurtzite GaN/AlN nanodiscs as evidenced by a reduction of the exciton lifetimes by up to four orders of magnitude. Furthermore, the tapered geometry of the utilized nanowires (which embed the investigated IFGARD nanodiscs) facilitates the experimental differentiation between quantum confinement and Stark emission energy shifts. Due to the IFGARD, both effects become independently adaptable.

[1] Institut für Festkörperphysik, Technische Universität Berlin, Hardenbergstr. 36, 10623 Berlin, Germany. [2] Bundesanstalt für Materialforschung und -prüfung (BAM), 12200 Berlin, Germany. [3] Institut für Festkörperphysik, Universität Bremen, Otto-Hahn-Allee 1, 28359 Bremen, Germany. [4] I. Physikalisches Institut, Justus-Liebig-Universität Giessen, Heinrich-Buff-Ring 16, 35392 Giessen, Germany. [5] Institute of Physics, École Polytechnique Fédérale de Lausanne (EPFL), CH-1015 Lausanne, Switzerland. Correspondence and requests for materials should be addressed to S.S. (email: sarah-schlichting@hotmail.de) or to G.M.O.Hön. (email: gerald.hoenig@physik.tu-berlin.de)

Group-III-nitride semiconductors are key materials for visible and ultraviolet light-emitting diodes, laser diodes[1,2], and quantum-light sources[3–5]. In particular GaN as well as AlN favorably crystalize in the wurtzite crystal structure[6]. Hence, heterostructures based on these materials suffer from a strong electric field induced by a piezo- and pyroelectric polarization parallel to the most natural crystal growth direction [0001], the so called *c*-axis[7–10]. The polarization-induced internal fields cause a redshift of the exciton emission energy inside these heterostructures, known to be the prominent feature of the quantum-confined Stark effect (QCSE)[11–15], which is accompanied by a drastic decrease of the spatial electron-hole overlap in the direction of the *c*-axis[3,8,16–25]. Different approaches to eliminate or to diminish the electric field across the optically active region in group-III-nitride heterostructures have been investigated, such as growth on non- or semi-polar crystal planes[26,27], forcing the growth of the cubic zincblende phase[28], or the screening of the fields with doping-induced free carriers[29]. Generally, approaches to avoid the preferential [0001] wurtzite crystal growth are challenging as they often produce a reduced crystal quality frequently combined with comparably lower deposition rates[30–35]. A more promising method to control the internal electric field is the Internal-Field-Guarded-Active-Region Design (IFGARD)[36], theoretically developed by Hönig et al.[37]. As described in detail in ref. [37], a conventional structure of a GaN quantum well (QW) embedded in AlN barriers is complemented in the IFGARD structure by additional GaN guard layers enclosing the AlN barriers (see Fig. 1a–c). This is not intuitive as the additional GaN guard layers reabsorb a certain percentage of the photons generated in the QW. But as discussed by Hönig et al.[37], the overall gain based on the elimination of the polarization field in the QW and the resulting boost in the exciton recombination probability can overcompensate the reabsorption losses by the guard layers, if the thickness of the guard layer in the emission direction is below the emitted wavelength[38–40]. It was numerically demonstrated that this concept leads to a constant piezo- and pyroelectric polarization potential inside of a QW, which results in flat conduction- and valence-band edges therein (Fig. 1c). This elimination of the electric field inside the QW yields a higher spatial overlap of the electron and hole wave function, and hence a drastic rise of the exciton recombination probability. As calculated in ref. [37], this maximized exciton recombination probability implicates a gain in the number of emitted photons per unit second by two orders of magnitude.

It is important to note that the IFGARD approach does not require a change in the underlying growth procedure; hence, no degradation of the crystal quality occurs as frequently observed for non- and semi-polar growth. Maintaining the initial crystal growth method and substrate material is a big advantage of the present concept compared to any other alternative approaches that aim to reduce or even eliminate the internal polarization fields in semiconductor heterostructures[30–35].

In this work, we show the successful implementation of the IFGARD concept for the example of nanowires (NWs) containing GaN nanodiscs (NDs). In particular, we demonstrate the reduction of the internal electric field inside of the GaN NDs down to zero, which reveals the immense advantage of the IFGARD over alternative, more conservative design concepts. Furthermore, we identify the individual contributions of the pure QCSE and the pure confinement effect based on two sample series with varying barrier and ND thickness.

Results

Sample description. The investigated NWs were grown by plasma-assisted molecular beam epitaxy ($T_{\mathrm{substrate}} = 790\,°\mathrm{C}$, $T_{\mathrm{Ga}} = 916\,°\mathrm{C}$, $T_{\mathrm{Al}} = 1069\,°\mathrm{C}$) on Si (111) substrates[19,29]. Figure 1 illustrates the GaN NWs (Fig. 1a, b) with the corresponding band profiles along the growth axis (Fig. 1c) as well as corresponding scanning transmission electron microscopy (STEM) images (Fig. 1d). The STEM images were recorded with a HAADF (high-angle annular dark field) detector showing single NWs with 1-nm-thick AlN barriers (left, black) and 6-nm-thick AlN barriers (right, black) at a constant ND (white) thickness of 4 nm.

The NWs grow along the polar [000-1] axis of the wurtzite crystal structure. Each NW embeds a stack of 40 GaN NDs separated by AlN barriers. The first GaN guard layer has a length of 650 nm in growth direction that corresponds to the growth of a well-established GaN NW template with high crystalline quality. The NW ends with a 20-nm-thick GaN guard layer (Fig. 1a, b) in order to realize the fundamental IFGARD symmetry assuring sufficient transparency and coverage for all nanowires across our sample. It is important to underline that the most simplistic stack element consists of one AlN barrier followed by one GaN ND[37]. This stack element is repeated for 40 times in order to clearly separate the ND from the guard layer signal. This sequence is encapsulated by the aforementioned GaN guard layers. In total, the NWs have a length of up to 1 µm.

The formation of an AlN shell and an increasing diameter of successively grown GaN NDs is observed due to the significant lateral growth of AlN (compare Fig. 1d)[41]. Consequently, the NWs exhibit a tapered shape[42] with the diameter increasing from 28 to 36 nm for the NWs with 1-nm-thick AlN barriers (Fig. 1d, left) and from 38 to 74 nm for the NWs with 6-nm-thick AlN barriers (Fig. 1d, right). Considering the conservation of a constant interface-charge density, the particularly tapered shape leads to different net interface charges (red+, blue—signs in Fig. 1a, b) at either side of each AlN barrier: the top interface to the GaN is larger than the interface to the GaN below each AlN barrier. This total interface-charge discrepancy is the perfect feature to proof the influence of the IFGARD on the electric field within the NDs, as in this case the flatness of the band-edge (Fig. 1c) depends on the barrier thickness—a situation similar to what Hönig et al. discussed in ref. [37] for IFGARD-based quantum dots. Hence, it becomes possible to control the built-in electric field in the NDs by adjusting the AlN barrier thickness and thus the net interface charges. Furthermore, thicker AlN barriers lead to an enhanced lateral dimension, which evokes a more pronounced tapering of such NWs with thicker AlN barriers, further enhancing their built-in electric field strengths. The angle α of the tapered NW, delineated in Fig. 1b, gets smaller with reduced AlN barrier thickness until the tapered-shape turns into a straight shape (Fig. 1a vs. 1b, compare Fig. 1d). Consequently, we produced two sample series: (i) samples with decreasing AlN barrier thickness from 6 to 1 nm with a constant GaN ND thickness of 4 nm and (ii) samples with a constant AlN barrier thickness of 1 nm and GaN ND thicknesses of 1, 2, and 3 nm. Since a ND thickness of 4 nm is large compared to the exciton-Bohr radius in GaN (effective Bohr radius $a^* = \frac{m_e}{m^*}\varepsilon_r a_0 \le 3\,\mathrm{nm}$)[3,43–47], we would expect an emission energy (without built-in electric fields) close to the free-exciton transition energy in bulk GaN of approximately 3.48 eV at cryogenic temperatures[48,49]. Hence, decreasing the thickness of the AlN barriers is expected to blueshift the ND emission towards the free-exciton transition energy in bulk material by reducing the internal electric fields in the NDs. After having counteracted the QCSE by the discussed IFGARD structure with minimal barrier widths, we tune the energy to even higher energies by confining the excitons in thinner NDs.

Photoluminescence behavior. Figure 2 displays µ-PL spectra, which are recorded with an excitation power of 15 µW at a

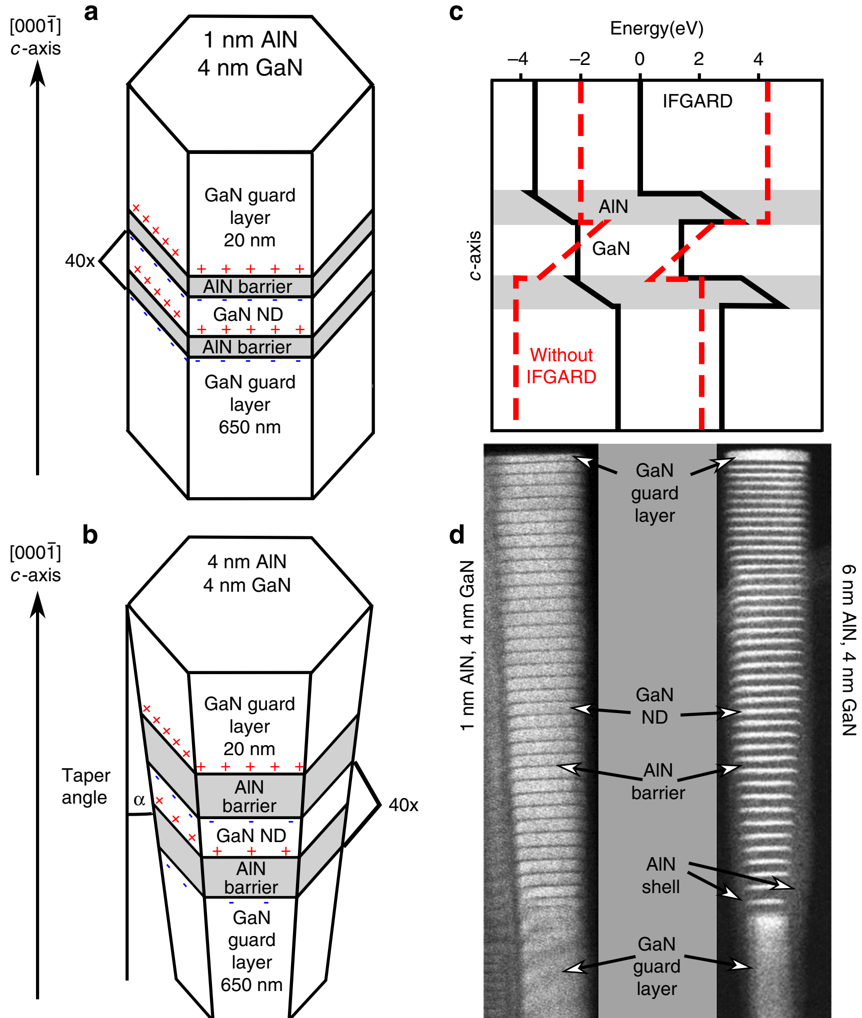

Fig. 1 Schematic sketch of nanowires (NWs) with embedded IFGARD nanodiscs with AlN barriers of 1 nm (**a**) and 4 nm (**b**) thickness. NWs with an increased barrier thickness are accompanied by an increased taper angle α due to lateral growth of the barrier material. Red + and blue - signs mark the positions of interface charges induced by the wurtzite crystal polarization. Due to the taper angle α of the NWs (**b**), the individual net interface charges of each AlN-barrier interface differ. In **c**, a sketch of the black IFGARD band profile is compared to the corresponding conventional nanodisc band profile in red. **d** shows HAADF-STEM images of the stacked GaN/AlN nanodiscs with 1 nm (left) and 6 nm barriers (right)

temperature of 7 K. 15 μW excitation-power spectra are chosen for this plot as they represent a trade-off between energetically well separated luminescence maxima for all samples with sufficient intensity to be plotted on a linear scale (compare the yellow bar in Fig. 3). The spectra are not normalized and therefore quantitatively comparable in absolute intensities. Please note that the excitation power of 15 μW does not represent the lowest applied power (marked by a green bar in Fig. 3). Effects regarding the samples' reflectance and light extraction efficiency due to the nanowire-geometry changes, as well as the changed volume-filling factors of the NDs within the excitation spots have not been taken into account for the creation of Fig. 2. Hence, the changes of intensities in Fig. 2 are dominated, but not exclusively caused by the change of the electron–hole overlaps in the samples. Besides the dominant ND emission signature, the luminescence band of the bulk-like GaN guard layers—close to the free-exciton emission energy in bulk GaN 3.48 eV[48,49]—is visible and marked in Fig. 2 by the dashed, blue line. As shown in Fig. 2, the emission peak energy of the GaN NDs in the QCSE regime (GaN ND thickness is constant at 4 nm with varied AlN-barrier thickness: 6, 4, 2, and 1 nm) shifts from 2.76 to 3.34 eV for decreased barrier thicknesses. This shift is accompanied by a strong increase in absolute luminescence intensity combined with a decrease in the full-width at half-maximum (FWHM) (750–75 meV) of the ND-luminescence peaks in Fig. 2 for decreasing barrier thicknesses.

For decreasing ND thicknesses an even further shift to higher emission energies from 3.34 to 4.04 eV occurs due to a stronger confinement of the charge carriers in the thinner NDs. At the same time, the absolute luminescence intensity decreases while the FWHM of the ND-luminescence peaks increases from 83 to 330 meV. The luminescence intensity decrease is caused by the reduced photon-absorption volume of the thinner NDs, while the stronger impact of monolayer-thickness variations in the thinner ND ensembles broadens the emission bands. As motivated at the beginning of this section, Fig. 2 was recorded with an increased excitation power of 15 μW causing a blue-shifted photoluminescence-peak position relative to the lowest pump powers in Fig. 3 due to partial screening of the QCSE by excited charge carriers[50–52]. The energetically smallest, measurable luminescence-peak positions are therefore displayed in Fig. 3. Figure 3 reveals the influence of the excitation-pump power (that was varied from 0.035 to 500 μW) on the emission-peak energy of the respective

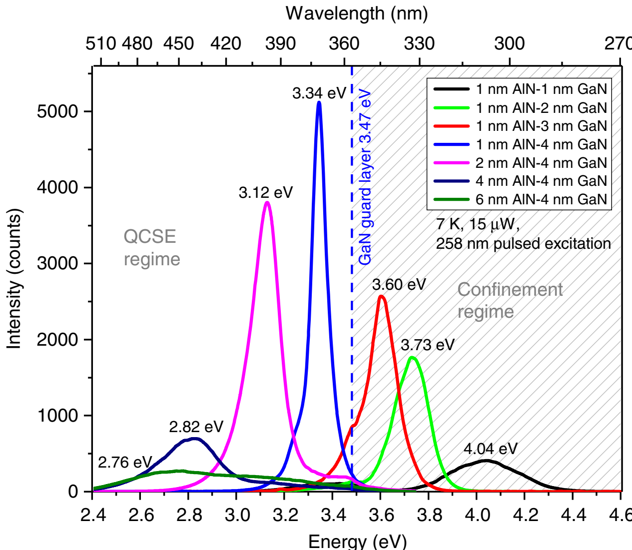

Fig. 2 Overview μ-PL spectra. The μ-PL spectra of all investigated samples are excited by a frequency-quadrupled, pulsed fiber laser with 258 nm wavelength and an excitation power of 15 μW at 7 K. For a fixed GaN ND thickness of 4 nm, the emission energy can be shifted by just varying the AlN barrier thickness from 6 nm down to 1 nm. A further reduction of the emission energy is achieved by reducing the ND thickness from 4 to 1 nm, while keeping the barrier thickness constant at 1 nm. In all samples, the dominant GaN ND luminescence is accompanied by the GaN guard layer luminescence (marked by the dashed, blue line), which divides the samples series into the so called QCSE regime and the confinement regime

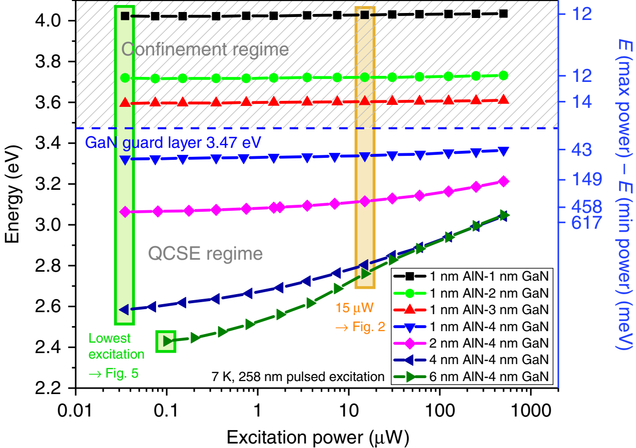

Fig. 3 Excitation power dependence of emission-peak positions. The emission peak positions of the nanodisc (ND) samples are plotted for excitation powers between 0.035 and 500 μW (measurement errors smaller than data point symbols). The total emission energy shift between the lowest (min) and highest (max) excitation power is given on the right, vertical axis (blue) representing the achieved polarization field screening by excited charge carriers for the QCSE regime and the effect of ND-band filling for the confinement regime

ND luminescence. On the right, vertical axis (blue) the emission energy shift is noted, representing the quantitative screening of the QCSE by the excited charge carriers plus a ND-band-filling effect converging for thinner NDs towards 12 meV. The gray shading visually divides Fig. 3 into a region either containing the results for IFGARD samples with a negligible QCSE (with total emission-energy shifts ≤14 meV) or those samples, whose emission characteristics are evidently affected by the QCSE. This gray shading is transferred to Fig. 2 including the notations: "QCSE" and "confinement regime". The energy range for which the QCSE dominates the emission properties is located below the bulk-like GaN luminescence of the guard layers. As visible in Fig. 3, the total emission-energy shift reduces with decreasing AlN-barrier widths from 617 meV (6 nm AlN barrier) to 43 meV (1 nm AlN barrier). The apparent trends for the intensity, the energy shifts and the evolution of the FWHM values are accompanied by corresponding changes in the exciton lifetimes.

The results of the μ-TRPL measurements are presented for all samples within the QCSE regime in Fig. 4a and for the samples within the confinement regime in Fig. 4b. As the transients exhibit a biexponential decay[53], the fit parameters, τ_1 and τ_2, are shown in the legends of Fig. 4a, b. These transients are recorded at the individual ND luminescence maxima and the dominant decay time (highest intensity in the temporal decay) for each sample is highlighted by bold letters in the legends. Remarkably, for a fixed GaN ND thickness of 4 nm, the decay time decreases by more than two orders of magnitude from (7.34 ± 0.10) μs for the thickest AlN barriers down to (40 ± 7) ns for its thinnest counterpart, as predicted for the IFGARD approach[37]. Subsequently, if one decreases the ND thickness (4–1 nm) for the samples with the thinnest AlN barrier of 1 nm, the decay time drops further down to approximately 0.7 ns for all three samples. All those samples that are part of the confinement regime feature very similar transients, presented in Fig. 4b.

Discussion

It is important to note that a 4-nm-thick GaN ND is not able to significantly quantum-confine excitons by its dimensions in absence of the QCSE[3,43,46,47]. Therefore, all IFGARD samples with an ND thickness of 4 nm would (without the tapering of the embedding NWs) emit at the same luminescence energy close to the free-exciton-emission energy of bulk GaN (3.48 eV[48,49]). Hence, applying the IFGARD in straight NWs (without any tapering) would perfectly annihilate the built-in field strengths and no tuning of the QCSE would be possible. The free-exciton emission energy is indicated by the luminescence of the bulk-like GaN guard layers in all recorded spectra and represents the transition between the QCSE and the confinement regime. In the confinement regime, the NDs show no indication of built-in fields and the overall energy shift to higher values for thinner NDs is solely caused by the quantum confinement without being affected by a counteracting QCSE redshift. This fact is demonstrated by the power-dependent μ-PL measurements analyzed in Fig. 3. Here, a screening of the internal electric field by excited charge carriers at high excitation powers becomes visible for the QCSE regime, only. The screened QCSE energy drastically reduces for decreasing AlN barrier thicknesses. Within the QCSE regime, the internal electric field strength is a consequence of two major effects: first, the unequally sized AlN–GaN interfaces due to the tapering of the NWs on either side of each AlN barrier lead to a non-zero net-polarization field inside of the NDs, similar to the IFGARD quantum dot case theoretically described by Hönig et al.[37] as the total number of space charges on both interfaces differ from each other. Second, the pronounced taper angle α (compare Fig. 1b) in the samples with thicker AlN barriers causes more unequal AlN–GaN interfaces further strengthening the net-polarization as explained in the first case. Besides, stronger strain due to thicker AlN barriers might contribute to a higher piezo-electric field strength. Nevertheless, we expect pseudomorphically strained AlN barriers not significantly influencing the strain within the NDs. Hence, the whole QCSE regime features a strong dependence of the ND luminescence energy on the AlN barrier

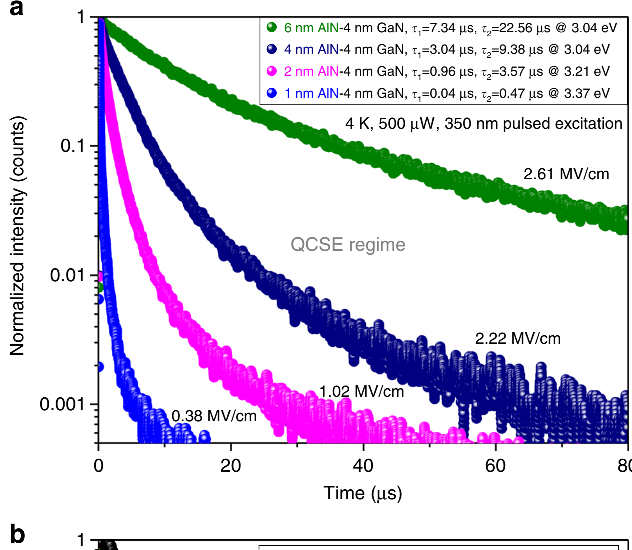

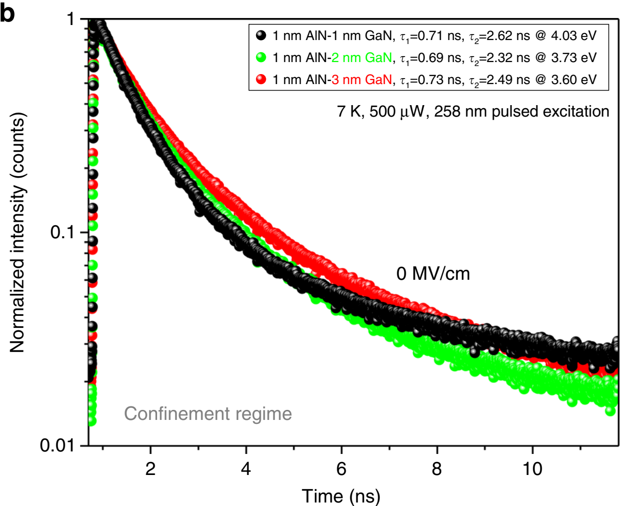

Fig. 4 Time-resolved μ-photoluminescence transients. The time-resolved μ-photoluminescence (μ-TRPL) transients of the samples within the QCSE regime shown in **a** reveal the decreasing exciton decay times due to smaller residual electric field strengths in samples with decreased barrier widths. **b** μ-TRPL transients of the samples within the confinement regime show a much smaller, constant decay time due to the eliminated electric field strength. The temporal resolution is better than 10 ps. The exciton lifetimes ($\tau_{1,2}$) for each biexponential decay are given in the legend; the dominant lifetime is always highlighted in bold. All μ-TRPL transients are recorded at the individual ND luminescence maxima

thickness as shown in Fig. 2 in addition to strong screening effects caused by enhanced excitation powers, cf. Fig. 3. Here, even the highest pump powers (already leading to a moderate sample degeneration under long-time exposure) cannot fully screen the built-in polarization fields in the samples with AlN barrier widths exceeding 1 nm—an observation similar to the unattainable full carrier screening in conventional GaN/AlN QW structures[29].

Decreasing the ND thickness further reduces the field strength within the NDs (compare Fig. 1a) as the finite lateral dimensions of the equally sized "capacitor plates" (due to the finite dimensions of the NWs) become less important. Therefore, the QCSE in the whole ND series becomes negligible, resulting in the convergence of the total energy shifts against 12 meV (visible in Fig. 3) indicating an ND-band-filling effect[54–56]. Hence, the overall emission-peak positions of the confinement regime samples in Fig. 2 are purely caused by quantum confinement in addition to an ND-band filling. This is similar to previous achievements for nonpolar GaN/AlN QWs[26,57–59], which still exhibit lower emission energies than the investigated IFGARD NDs. Besides the aforementioned influence of the decreasing QCSE on the spectra in Fig. 2, we obtain an increased overlap between the electron and hole occupation probability density, leading to an enhanced exciton-decay rate. In turn, this leads to a strong increase in absolute intensity for the samples with decreased AlN-barrier widths in the QCSE regime. Additionally, the decreased electric dipole moment of the exciton couples less efficiently to defect charge fluctuations in the ND vicinity, which is one mechanism that reduces the FWHM for the emission peaks of the samples related to the QCSE regime[16]. Furthermore, the 1-nm-thick AlN barriers and 4-nm-thick GaN NDs (Fig. 2, blue) exhibit multiple LO-phonon replicas ($E_{LO} = 94$ meV) whereas all samples within the confinement regime do not show any phonon replicas. While the visibility of multiple LO-phonon replicas implicates a large Huang-Rhys-factor and confirms the existence of built-in excitonic electric dipole moments[60] within the QCSE-regime NDs, their non-visibility for the confinement-regime NDs indicates the absence of a built-in excitonic electric dipole moment.

When the thickness of the NDs in the confinement regime is decreased, the emission energy even exceeds 4 eV due to the strong confinement in absence of the QCSE. The reduction of the absolute intensity (for a constant pump power) can straightforwardly be understood: As the number of NDs (40) is conserved, the photon-absorption volume is reduced. At the same time, the FWHM of the NDs' luminescence peaks within the confinement regime rises. This can be understood considering our quantitative STEM analysis showing random ND-thickness fluctuations of ±1 monolayer thickness that have the strongest impact on the confinement energy of the excitons within the thinnest NDs[61].

After having separated the QCSE from the confinement effect, the remaining internal electric field strength can be estimated for individual NDs of the QCSE regime simply by the energetic difference between the GaN-guard-layer-luminescence energy and the respective ND emission energy. This difference represents the energy of the electric dipole moment of one exciton in the built-in polarization field. As shown by Nakaoka et al.[62], the quadratic polarizability of the exciton is only of relevance for electric field strengths up to 100 kV cm^{-1}, causing energetic shifts of up to 3 meV. Therefore, we can safely neglect the polarizability of the ND exciton and roughly approximate it by a solid electric dipole moment. Here, we estimate the maximal possible dipole moment μ_z by the thickness of the NDs times the elemental charge e, being $\mu_z \approx 4\,\text{nm}\cdot e$ for the QCSE regime[63]. Hence, the energetic luminescence offset to the 3.47 eV of the bulk-like GaN guard layers $E_{GaN} - E_{ND} = \mu_z F_z$[64] has to be divided by μ_z to give a simple approximation of the built-in field strength, which is noted in Fig. 5. This approximation should become more reliable for higher field strengths, as the true electric dipole moment of the exciton converges towards the approximated $4\,\text{nm}\cdot e$ with higher field strengths. By the use of this rather empiric method, a mean value for the built-in field strength of approximately 10,000 NDs in the excitation spot is derived, which averages out the influence of possible QW-thickness fluctuations and strain gradients within the tapered nanowires by evaluating the emission energies of the luminescence maxima only. For a better understanding of the luminescence distribution, numeric strain studies of tapered nanowires including all layers in three dimensions are necessary, which is beyond the scope of this publication. Nevertheless, the estimated 2.61 MV cm^{-1} in the IFGARD QW with 6 nm AlN barriers are still more than two times smaller than the field strengths in comparably thick conventional GaN/AlN QWs[25,65]. Although this discrepancy might lead to the

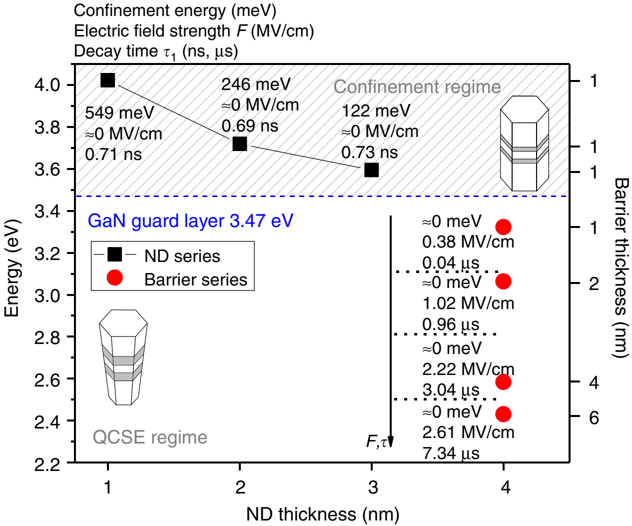

Fig. 5 Results summary. The graphical overview summarizes the main results of this work and illustrates the correlation between barrier and nanodisc (ND) thicknesses, the ND emission energies (within the confinement regime, marked by black squares and the QCSE regime by red dots), the unscreened electrical field strengths (MV cm^{-1}), the exciton confinement energies (meV), and the dominant decay times (ns, µs). Additionally, the geometric nanowire structure in the respective regimes is indicated

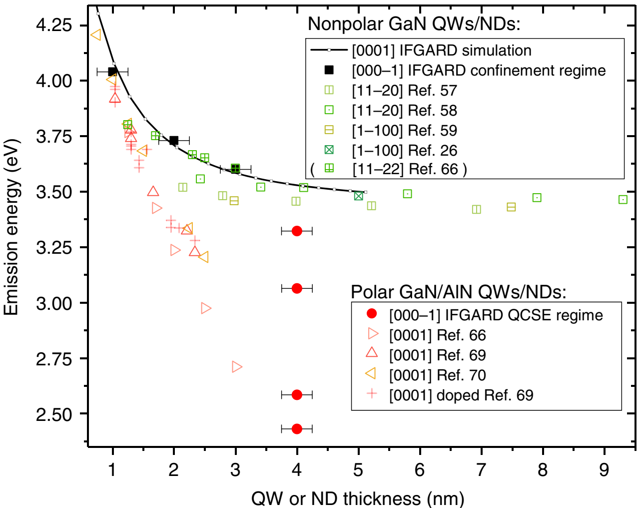

Fig. 6 Literature data compilation. Direct comparison of the experimentally determined emission energies for the different nanodisc (ND) samples in the confinement regime (black squares) and the QCSE regime (red dots) to numeric results for GaN/AlN IFGARD quantum wells (QWs, black line) exhibiting totally shielded polarization fields (built-in field strength = 0 MV cm^{-1}). Error bars represent ND-thickness fluctuations of one monolayer GaN. Published values for pure GaN QWs with nonpolar growth directions are included as green squares[26,57–59,67] and confirm the converging trend that is predicted for GaN QWs without built-in fields. While the conventionally grown [0001], fully polar GaN/AlN QWs[67–69] (red triangles) emit at much lower emission energies for well widths exceeding 1 nm. Even doping in the order of 5×10^{19}cm^{-3} (red crosses) does not significantly alter the emission energies of the polar GaN/AlN QWs

assumption of smaller electric dipole moments, i.e., $\mu_z < 2$ nm·e this would be unrealistically small for a 4-nm-thick ND, demonstrating the IFGARD effectively reducing the field strength in all samples. Moreover, the overall decrease of the decay time from 7.34 µs down to 0.7 ns (in Fig. 4) correlates with the decreasing electric field strength of the NDs from **a** 2.61 MV cm^{-1} over 0.38 MV cm^{-1} down to approximately zero for the whole confinement regime **b** with a constant effective decay time of approximately 0.7 ns. Figure 5 summarizes all discussed results: As expected, for a pure confinement effect[26,57–59,66], the luminescence energies (black squares) in the confinement regime converge towards the bulk-like GaN-guard-layer luminescence energy of 3.47 eV.

A comparison of the experimentally determined emission energies of the NDs to numeric 1D simulations of perfectly shielded IFGARD GaN/AlN QWs (without built-in polarization fields) is given in Fig. 6 (black line) along with a compilation of experimental literature values. As already discussed, for diminishing confinement the simulated emission energies converge towards the bulk GaN emission energy as it is observed for the confinement regime samples (black squares), with their emission energies being in perfect agreement with the predicted ones. This converging behavior was previously only observed in studies of nonpolar GaN QW samples (green squares), while prior studies on c-plane, strongly polar GaN/AlN QWs (red triangles) reported an approximately linear emission energy dependence with respect to the QW width. Hence, Fig. 6 evidences that IFGARD is capable of achieving luminescence shifts for a c-plane heterostructure that can otherwise only be achieved by cumbersome, nonpolar growth!

Interestingly, any doping of the QWs on the order of 5×10^{19} cm^{-3} (red crosses) does not have a significant effect on the QCSE if compared to the offset between polar and nonpolar samples. Overall, the comparison proves the absence of built-in polarization fields in the IFGARD samples within the confinement regime. Unfortunately, as we had no access to pure AlN nanowires, we are not able to compare the investigated IFGARD NDs directly to "conventional" ND structures; but, Fig. 6 depicts a comparison between our results and a wide range of examples from the literature. Comparing an IFGARD QW (grown on a GaN substrate) to a conventional GaN QW grown on whatever substrate and embedded in an AlN matrix should result in the same emission energy offset as it is visible between the nonpolar and polar samples in Fig. 6. Nevertheless, such IFGARD QWs, as already discussed, would not allow the gradual QCSE tuning (red dots), we showed in this paper to emphasize our claim of the first experimental proof of the IFGARD.

Finally, it is important to understand that the (111)Si–(0001) GaN interface is expected to build up space charges at the bottom of the NWs. The resulting net-bottom-interface charge causes a field strength that strongly diminishes over the 650 nm distance of the IFGARD-ND stack according to $F \sim \frac{1}{r^3}$ and has therefore only a negligible influence on the entire ND luminescence. This point-charge approximation would not be valid for IFGARD QWs, where the distance to the wafer interface would be small if compared to the wafer diameter. Hence, in such QW samples the bottom hetero-interface should be avoided, e.g., by homo-epitaxial growth or a subsequent laser lift-off process[67], seeking to reestablish the fundamental symmetry of the IFGARD approach.

In summary, we experimentally demonstrate that the IFGARD represents a beneficial method to suppress the internal electric fields in polar heterostructures such as ND structures. As a result, the QCSE is eliminated as approved by the presented shift of the emitted photons to higher energies (in comparison to conventional QWs with equal thickness) and by an enhanced oscillator strength that causes a distinct intensity boost and a decrease of decay times by more than two orders of magnitude for NDs with constant thickness. Furthermore, we show that in the presented tapered NW structures, the internal electric field becomes

adjustable by the thickness of the AlN barriers. Therefore, the IFGARD opens the possibility to effectively tune the QCSE in polar semiconductor heterostructures without the need for the growth of extraordinary phases or epitaxy on nonpolar crystal planes. Based on this flexibility, IFGARD allows to utilize comparably thick QWs without sacrificing a large electron–hole overlap for efficient photon generation by overcoming the detrimental effects of the QCSE[55].

Methods

The optical properties of the NDs were investigated by micro-photoluminescence (μ-PL) and time-resolved μ-PL (μ-TRPL) measurements, the latter with two different experimental setups to explore the exciton lifetimes from the ps- up to the μs-range. The samples were mounted into a helium-flow cryostat providing temperatures down to 5 K.

In the μ-PL setup, the randomly distributed, standing as-grown NWs were excited by a pulsed (76 MHz repetition rate and 2 μm spot size illuminating approx. 250 NWs) frequency-quadrupled, 5 ps pulse width fiber laser resulting in an excitation wavelength of 258 nm. The spectra were dispersed in a 0.85 m single monochromator by a 150 lines/mm grating (500 nm blaze wavelength). The photons were detected with an UV-enhanced Si-charge-coupled device (CCD) array. All spectra were calibrated with an Hg-lamp and are corrected for the refractive index of air. μ-TRPL measurements in the ps- to ns-range were performed with the same laser as used for the μ-PL measurements, here coupled into a subtractive 0.35 m double monochromator with 2400 lines/mm gratings as dispersing elements (300 nm blaze wavelength). The time-correlated single-photon-counting technique is used in combination with a hybrid photomultiplier detector assembly for recording the temporal decays with a temporal resolution of better than 10 ps.

The μs-range TRPL measurements are performed with a pulsed dye laser (350 nm, 100 Hz, 12 ns pulse width) pumped by a 308 nm XeCL-Excimer laser (100 Hz, 15 ns pulse width). As a dye we employed 2-methyl-5-t-butyl-*p*-quaterphenyl as active medium dissolved in 1,4-dioxane for spectroscopic purposes. For the dispersion an additive double monochromator with a focal length of 1 m and a holographic 1800 lines/mm grating are used. For recording the PL transients, a multichannel-plate photomultiplier with an S20 cathode combined with time-correlated single-photon-counting and multi-channel-scaling technique (including multi-stop capability) are utilized. The recorded temporal decays are all corrected for the specific response characteristics of the respective setup[68].

Please note that the nanowire samples were investigated as grown without any processing as a forest of standing nanowires. Therefore, all results have been recorded at ensembles of nanowires, comprising nanowires that each contained 40 NDs.

Data availability. All data generated or analyzed during this study are included in this published article and its Supplementary Data file.

Received: 20 February 2018 Accepted: 11 July 2018
Published online: 23 August 2018

References

1. Gil, B. *III-Nitride Semiconductors and their Modern Devices* 1st edn (Oxford University Press, Oxford, 2013).
2. Nakamura, S., Pearton, S. & Fasol, G. *The Blue Laser Diode. The Complete Story*. 2nd updated and extendeded edition (Springer-Verlag, Berlin, Heidelberg, New York, 2013).
3. Hönig, G. et al. Manifestation of unconventional biexciton states in quantum dots. *Nat. Commun.* **5**, 5721 (2014).
4. Callsen, G. et al. Steering photon statistics in single quantum dots: from one- to two-photon emission. *Phys. Rev. B* **87**, 245314 (2013).
5. Holmes, M. et al. Measurement of an exciton Rabi rotation in a single GaN/Al (x)Ga(1-x)N nanowire-quantum dot using photoluminescence spectroscopy: evidence for coherent control. *Phys. Rev. Lett.* **111**, 057401 (2013).
6. Schliwa, A., Hönig, G. & Bimberg, D. in *Multi-Band Effective Mass Approximations* 1st edn (eds Ehrhardt, M. & Koprucki, T.) 57–86 (Springer, Cham, Heidelberg, New York, Dordrecht, London) (2014).
7. Ambacher, O. et al. Pyroelectric properties of Al (In) GaN/GaN hetero-and quantum well structures. *J. Phys. Condens. Matter* **14**, 3399 (2002).
8. Langer, R. et al. Giant electric fields in unstrained GaN single quantum wells. *Appl. Phys. Lett.* **74**, 3827 (1999).
9. Bernardini, F. & Fiorentini, V. Macroscopic polarization and band offsets at nitride heterojunctions. *Phys. Rev. B* **57**, R9427(R) (1998).
10. Ambacher, O. et al. Role of apontaneous and piezoelectric polarization induced effects in group-III nitride based heterostructures and devices. *Phys. Status Solidi B* **216**, 381–389 (1999).
11. Leroux, M. et al. Quantum confined Stark effect due to built-in internal polarization fields in (Al,Ga)N/GaN quantum wells. *Phys. Rev. B* **58**, R13371 (R) (1998).
12. Grandjean, N. et al. Built-in electric-field effects in wurtzite AlGaN/GaN quantum wells. *J. Appl. Phys.* **86**, 3714 (1999).
13. Nakaoka, T., Kako, S. & Arakawa, Y. Quantum confined Stark effect in single self-assembled GaN/AlN quantum dots. *Phys. E* **32**, 148 (2006).
14. Cingolani, R. et al. Spontaneous polarization and piezoelectric field in GaN/Al0.15Ga0.85N quantum wells: impact on the optical spectra. *Phys. Rev. B* **61**, 2711 (2000).
15. Fiorentini, V., Bernardini, F., Della Sala, F., Di Carlo, A. & Lugli, P. Effects of macroscopic polarization in III-V nitride multiple quantum wells. *Phys. Rev. B* **60**, 8849 (1999).
16. Kindel, C. et al. Spectral diffusion in nitride quantum dots: emission energy dependent linewidths broadening via giant built-in dipole moments. *Phys. Status Solidi (RRL)* **8**, 408–413 (2014).
17. Kako, S., Miyamura, M., Tachibana, K., Hoshino, K. & Arakawa, Y. Size-dependent radiative decay time of excitons in GaN/AlN self-assembled quantum dots. *Appl. Phys. Lett.* **83**, 984 (2003).
18. Renard, J. et al. Evidence for quantum-confined Stark effect in GaN/AlN quantum dots in nanowires. *Phys. Rev. B* **80**, 121305(R) (2009).
19. Müßener, J. et al. Probing the internal electric field in GaN/AlGaN nanowire heterostructures. *Nano Lett.* **14**, 5118–5122 (2014).
20. Kindel, C. et al. Exciton fine-structure splitting in GaN/AlN quantum dots. *Phys. Rev. B* **81**, 241309(R) (2010).
21. Ostapenko, I. A. et al. Large internal dipole moment in InGaN/GaN quantum dots. *Appl. Phys. Lett.* **97**, 063103 (2010).
22. Bretagnon, T. et al. Radiative lifetime of a single electron-hole pair in GaN/AlN quantum dots. *Phys. Rev. B* **73**, 113304 (2006).
23. Bretagnon, T. et al. Time dependence of the photoluminescence of GaN/AlN quantum dots under high photoexcitation. *Phys. Rev. B* **68**, 205301 (2003).
24. Fiorentini, V., Bernardini, F. & Ambacher, O. Evidence for nonlinear macroscopic polarization in III–V nitride alloy heterostructures. *Appl. Phys. Lett.* **80**, 1204 (2002).
25. Adelmann, C. et al. Growth and optical properties of GaN/AlN quantum wells. *Appl. Phys. Lett.* **82**, 4154 (2003).
26. Waltereit, P. et al. Nitride semiconductors free of electrostatic fields for efficient white light-emitting diodes. *Nature* **406**, 865–868 (2000).
27. Paskova, T. *Nitrides with Nonpolar Surfaces: Growth, Properties, and Devices. Nitrides with Nonpolar Surfaces: Growth, Properties, and Devices*. 1st edn (WILEY-VCH, Weinheim, 2008)
28. Paisley, M. J., Sitar, Z., Posthill, J. B. & Davis, R. F. Growth of cubic phase gallium nitride by modified molecular-beam epitaxy. *J. Vac. Sci. Technol. A* **7**, 701 (1989).
29. Hille, P. et al. Screening of the quantum-confined Stark effect in AlN-GaN nanowire superlattices by germanium doping. *Appl. Phys. Lett.* **104**, 102104 (2014).
30. Kemper, R. M. et al. Anti-phase domains in cubic GaN. *J. Appl. Phys.* **110**, 123512 (2011).
31. Bürger, M. et al. Lasing properties of non-polar GaN quantum dots in cubic aluminum nitride microdisk cavities. *Appl. Phys. Lett.* **103**, 021107 (2013).
32. Kako, S. et al. Single-photon emission from cubic GaN quantum dots. *Appl. Phys. Lett.* **104**, 011101 (2014).
33. Schupp, T. et al. Zinc-blende GaN quantum dots grown by vapor-liquid-solid condensation. *J. Cryst. Growth* **323**, 286–289 (2011).
34. Sergent, S., Kako, S., Bürger, M., As, D. J. & Arakawa, Y. Narrow spectral linewidth of single zinc-blende GaN/AlN self-assembled quantum dots. *Appl. Phys. Lett.* **103**, 151109 (2013).
35. Farrell, R. M., Young, E. C., Wu, F., DenBaars, S. P. & Speck, J. S. Materials and growth issues for high-performance nonpolar and semipolar light-emitting devices. *Semicond. Sci. Technol.* **27**, 024001 (2012).
36. Pahn, G. M. O., Callsen, G. & Hoffmann, A. Semiconductor device having an internal-field-guarded active region. International Patent Publication Number WO2017/042368 A1 (2017).
37. Hönig, G. M. O., Westerkamp, S., Hoffmann, A. & Callsen, G. Shielding electrostatic fields in polar semiconductor nanostructures. *Phys. Rev. Appl.* **7**, 024004 (2017).
38. Vico Triviño, N. et al. High quality factor two dimensional GaN photonic crystal cavity membranes grown on silicon substrate. *Appl. Phys. Lett.* **100**, 071103 (2012).
39. Chávez-Ángel, E. et al. Reduction of the thermal conductivity in free-standing silicon nano-membranes investigated by non-invasive Raman thermometry. *APL Mater.* **2**, 012113 (2014).

40. Muth, J. F. et al. Absorption coefficient, energy gap, exciton binding energy, and recombination lifetime of GaN obtained from transmission measurements. *Appl. Phys. Lett.* **71**, 2572 (1997).
41. Furtmayr, F. et al. Carrier confinement in GaN/Al(x)Ga(1−x)N nanowire heterostructures (0<x<1). *Phys. Rev. B* **84**, 205303 (2011).
42. Songmuang, R., Ben, T., Daudin, B., González, D. & Monroy, E. Identification of III–N nanowire growth kinetics via a marker technique. *Nanotechnology* **21**, 295605 (2010).
43. Banyai, L., Hu, Y. Z., Lindberg, M. & Koch, S. W. Third-order optical nonlinearities in semiconductor microstructures. *Phys. Rev. B* **38**, 8142–8153 (1988).
44. Shan, W., Xie, X. C., Song, J. J. & Goldenberg, B. Time-resolved exciton luminescence in GaN grown by metalorganic chemical vapor deposition. *Appl. Phys. Lett.* **67**, 2512 (1995).
45. Im, J. S. et al. Radiative carrier lifetime, momentum matrix element, and hole effective mass in GaN. *Appl. Phys. Lett.* **70**, 631 (1997).
46. Efros, A. L. in *Selected Papers on Semiconductor Quantum Dots, SPIE Milestone Ser.* Vol. 180 (ed. Wise, F. W.) 71 (SPIE. The international society for optics and photonics, Bellingham, Washington 2005).
47. Que, W. Excitons in quantum dots with parabolic confinement. *Phys. Rev. B* **45**, 11036–11041 (1992).
48. Volm, D. et al. Exciton fine structure in undoped GaN epitaxial films. *Phys. Rev. B* **53**, 16543 (1996).
49. Korona, K. P. Dynamics of excitonic recombination and interactions in homoepitaxial GaN. *Phys. Rev. B* **65**, 235312 (2002).
50. Reale, A. et al. Comprehensive description of the dynamical screening of the internal electric fields of AlGaN/GaN quantum wells in time-resolved photoluminescence experiments. *J. Appl. Phys.* **93**, 400 (2003).
51. Della Sala, F. et al. Free-carrier screening of polarization fields in wurtzite GaN/InGaN laser structures. *Appl. Phys. Lett.* **74**, 2002 (1999).
52. Kuokstis, E. et al. Polarization effects in photoluminescence of C-and M-plane GaN/AlGaN multiple quantum wells. *Phys. Rev. Lett.* **81**, 4130 (2002).
53. Beeler, M. et al. Long-lived excitons in GaN/AlN nanowire heterostructures. *Phys. Rev. B* **91**, 205440 (2015).
54. Casey, H. C. Jr., Muth, J., Krishnankutty, S. & Zavada, J. M. Dominance of tunneling current and band filling in InGaN/AlGaN double heterostructure blue light-emitting diodes. *Appl. Phys. Lett.* **68**, 2867 (1996).
55. Nippert, F. et al. Polarization-induced confinement of continuous hole-states in highly pumped, industrial-grade, green InGaN quantum wells. *J. Appl. Phys.* **119**, 215707 (2016).
56. Burstein, E. Anomalous optical absorption limit in InSb. *Phys. Rev.* **93**, 632 (1954).
57. Craven, M. D., Waltereit, P., Speck, J. S. & Denbaars, S. P. Well-width dependence of photoluminescence emission from a-plane GaN/AlGaN multiple quantum wells. *Appl. Phys. Lett.* **84**, 496–498 (2004).
58. Koida, T. et al. Improved quantum efficiency in nonpolar (11-20) AlGaN/GaN quantum wells grown on GaN prepared by lateral epitaxial overgrowth. *Appl. Phys. Lett.* **84**, 3768–3770 (2004).
59. Bhattacharyya, A. et al. Comparative study of GaN/AlGaN MQWs grown homoepitaxially on (1100) and (0001) GaN. *J. Cryst. Growth* **251**, 487–493 (2003).
60. Callsen, G. et al. Analysis of the exciton–LO-phonon coupling in single wurtzite GaN quantum dots. *Phys. Rev. B* **92**, 235439 (2015).
61. Rigutti, L. et al. Origin of energy dispersion in Al(x)Ga(1−x)N/GaN nanowire quantum discs with low Al content. *Phys. Rev. B* **82**, 235308 (2010).
62. Nakaoka, T., Kako, S. & Arakawa, Y. Unconventional quantum-confined Stark effect in a single GaN quantum dot. *Phys. Rev. B* **73**, 121305(R) (2006).
63. Hönig, G. M. O. Mehrteilchenzustände in Halbleiter-Quantenpunkten. PhD. Technische Universität Berlin. https://doi.org/10.14279/depositonce-4443 (2015).
64. Hönig, G. et al. Identification of electric dipole moments of excitonic complexes in nitride-based quantum dots. *Phys. Rev. B* **88**, 045309 (2013).
65. Pal, J., Tse, G., Haxha, V., Migliorato, M. A. & Tomić, S. Second-order piezoelectricity in wurtzite III-N semiconductors. *Phys. Rev. B* **84**, 085211 (2011).
66. Lahourcade, L. et al. Interband and intersubband optical characterization of semipolar ($11\bar{2}2$)-oriented GaN/AlN multiple-quantum-well structures. *Appl. Phys. Lett.* **93**, 111906 (2008).
67. Hahn, B., Galler, B. & Engl, K. Development of high-efficiency and high-power vertical light emitting diodes. *Jpn. J. Appl. Phys.* **53**, 100208 (2014).
68. O'Connor, D. V., Ware, W. R. & Andre, J. C. Deconvolution of fluorescence decay curves. A critical comparison of techniques. *J. Phys. Chem.* **83**, 1333–1343 (1979).
69. Tchernycheva, M. et al. Systematic experimental and theoretical investigation of intersubband absorption in GaN/AlN quantum wells. *Phys. Rev. B* **73**, 125347 (2006).
70. Kandaswamy, P. K. et al. GaN/AlN short-period superlattices for intersubband optoelectronics: a systematic study of their epitaxial growth, design, and performance. *J. Appl. Phys.* **104**, 093501 (2008).

Acknowledgements

We acknowledge support from the Deutsche Forschungsgemeinschaft (DFG) within the Collaborative Research Center 787 (CRC 787). J.M. acknowledges financial support from the JLU Gießen via the graduate scholarship.

Author contributions

S.S. wrote the manuscript, performed the measurements, and analyzed the presented data. S.S., G.H., and G.C. discussed and interpreted the data. G.H., G.C., and A.H. are the inventors of the IFGARD[38]. J.M., P.H., J.T, J.S., and M.E. developed the NDs in NW sample structure, produced the samples, and contributed to the overall data interpretation. S.W. contributed the IFGARD QW simulations in Fig. 6. T.G. and A.R. supplied the STEM analysis. G.H., G.C., A.H., and M.W. supervised the IFGARD project.

Additional information

Supplementary information accompanies this paper at https://doi.org/10.1038/s42005-018-0044-1.

Competing interests: The authors declare no competing Interests.

Reprints and permission information is available online at http://npg.nature.com/reprintsandpermissions/

Publisher's note: Springer Nature remains neutral with regard to jurisdictional claims in published maps and institutional affiliations.

Open Access This article is licensed under a Creative Commons Attribution 4.0 International License, which permits use, sharing, adaptation, distribution and reproduction in any medium or format, as long as you give appropriate credit to the original author(s) and the source, provide a link to the Creative Commons license, and indicate if changes were made. The images or other third party material in this article are included in the article's Creative Commons license, unless indicated otherwise in a credit line to the material. If material is not included in the article's Creative Commons license and your intended use is not permitted by statutory regulation or exceeds the permitted use, you will need to obtain permission directly from the copyright holder. To view a copy of this license, visit http://creativecommons.org/licenses/by/4.0/.

© The Author(s) 2018